



## Enhanced zonal trade winds warm the western South Atlantic surface during MIS 4 glacial descent

Ana Beatriz Pedrazzi-Chacon<sup>a,b,\*</sup>, Igor Martins Venancio<sup>a</sup>, Thiago Pereira dos Santos<sup>c</sup>, João Marcelo Ballalai<sup>a</sup>, Rodrigo Azevedo Nascimento<sup>d</sup>, Marília de Carvalho Campos<sup>e</sup>, Cristiano Mazur Chiessi<sup>c</sup>, Marilia Harumi Shimizu<sup>f</sup>, Ana Luiza Spadano Albuquerque<sup>b</sup>

<sup>a</sup> Programa de Pós-Graduação em Geociências (Geoquímica), Universidade Federal Fluminense, Niterói, Brazil

<sup>b</sup> Programa de Pós-Graduação em Dinâmica dos Oceanos e da Terra, Universidade Federal Fluminense, Niterói, Brazil

<sup>c</sup> School of Arts, Sciences and Humanities, University of São Paulo, São Paulo, Brazil

<sup>d</sup> Center for Marine Studies, Federal University of Paraná, Pontal do Paraná, Brazil

<sup>e</sup> Institute of Geosciences, University of Campinas, Campinas, Brazil

<sup>f</sup> General Coordination of Earth Science, National Institute for Space Research, São José dos Campos, Brazil

### ARTICLE INFO

Handling editor: Carin Andersson Dahl

### ABSTRACT

Marine Isotope Stage 4 (MIS 4, 70–60 ka BP) is commonly characterized by a rapid drop in global temperatures due to the establishment of glacial conditions. However, recent sea surface temperatures (SST) paleoclimatic records based on planktonic foraminiferal Mg/Ca ratios indicate a warming trend at the western margin of the South Atlantic during MIS 4. Here, we provide a compilation of Mg/Ca-based SST records from both the eastern and western margins of the South Atlantic, aiming to understand the main patterns and underlying mechanisms associated with the thermal evolution of the South Atlantic during MIS 4. Our results show that SST on the eastern margin of the South Atlantic followed the global cooling trend during the transition to MIS 4, while the western margin experienced warming during the same interval. We propose that the eastern-western thermal contrast observed in the first half of MIS 4 was caused by changes in the trade wind system. During the onset of MIS 4, a period of minimum Northern Hemisphere summer insolation led to an intensified trade wind zonal component and a weakened west African monsoon. This, in turn, strengthened the South Atlantic westward flowing currents, enhancing the transport of warm surface waters to the western margin. The intensified and more zonal southeastern trade winds increased eastern boundary upwelling, resulting in lower temperatures on the African margin. Our results highlight the importance of considering changes in the trade wind system in order to interpret the thermal responses of the South Atlantic during past glacial periods.

### 1. Introduction

The last glacial inception took place during the transition from Marine Isotope Stage 5 to 4 (MIS 5–4), ~70 ka BP. During MIS 4, global temperatures dropped rapidly, leading to the establishment of full glacial conditions around 60 ka BP. Furthermore, this period was characterized by significant surface ocean cooling, glacier and ice sheet expansion in the Southern Hemisphere, a significant sea-level drop (ca. 100m), a drawdown of atmospheric CO<sub>2</sub> and changes in ocean circulation (Cutler et al., 2003; Bereiter et al., 2012; Schaefer et al., 2015; Yu et al., 2016; Shackleton et al., 2021; Menking et al., 2022).

When comparing MIS 4 to other periods of full glacial conditions,

such as the Last Glacial Maximum (LGM; 23–19 ka BP), which occurred during the MIS 2 (29–14 ka BP), various similarities emerge, particularly regarding global temperatures (Osman et al., 2021; Shackleton et al., 2021). Atmospheric CO<sub>2</sub> levels recorded at the end of MIS 4 reached ~190 ppm, only ~5 ppm higher than the lowest concentrations reached during the LGM (Kohfeld and Chase, 2017). During MIS 4, in the high latitudes of the Southern Hemisphere, evidence based on diatoms indicates an increased duration of sea ice cover and the presence of ice in previously ice-free regions (Kohfeld and Chase, 2017). Furthermore, MIS 4 was marked by the development of more extensive glaciers in various glacial systems compared to MIS 2 (Schaefer et al., 2015; Doughty et al., 2021; Peltier et al., 2021). Both MIS 4 and the LGM show

\* Corresponding author. Programa de Pós-Graduação em Geociências (Geoquímica), Universidade Federal Fluminense, Niterói, Brazil.

E-mail address: [abpchacon@id.uff.br](mailto:abpchacon@id.uff.br) (A.B. Pedrazzi-Chacon).

concurrent cold conditions in the Northern and Southern Hemispheres as well as nearly absence of millennial-scale variability (Barker and Diz, 2014; Doughty et al., 2021; Shackleton et al., 2021).

Barker and Diz (2014) observed a sudden cooling of the southeast Atlantic during MIS 4 that coincided with decreases in temperature in Greenland and Antarctica. This simultaneous cooling in both hemispheres during the transition to glacial conditions in MIS 4 is further supported by the results of Doughty et al. (2021) and Shackleton et al. (2021). Meanwhile, published sea surface temperatures (SST) paleo-records based on planktonic foraminiferal Mg/Ca ratios from Santos et al. (2017), Venancio et al. (2018) and Nascimento et al. (2023) suggest a different pattern, indicating sustained warming at the western margin of the South Atlantic during MIS 4. These findings likely reflect regional oceanographic variability within the South Atlantic basin and challenge the notion that MIS 4 was a period of globally in-phase cold conditions.

Several parameters and mechanisms are generally associated with the thermal evolution of the global ocean between glacial and interglacial periods, among which the concentration of atmospheric CO<sub>2</sub> stands out. Variations in atmospheric CO<sub>2</sub> concentration affect Earth's radiative balance and, consequently, its climate (Sigman and Boyle, 2000). The role of CO<sub>2</sub> as an amplifier of temperature changes across glacial-interglacial cycles is well established (Adkins, 2013). In marine ecosystems, rising CO<sub>2</sub> levels are associated with ocean warming, changes in circulation and stratification, and shifts in nutrient and oxygen availability that affect primary productivity (Doney et al., 2012).

As pointed out by Kohfeld and Chase (2017), atmospheric CO<sub>2</sub> concentrations declined in three main phases during the last glacial cycle. Among these, the second phase (80–65 ka BP), which overlaps with our study interval, is particularly notable for its abrupt CO<sub>2</sub> drawdown (~40 ppm). This decline is linked to significant changes in the deep ocean circulation, specifically, a reduction in deep-water ventilation and an increase in surface ocean productivity, potentially stimulated by enhanced dust-borne nutrient input, both considered key mechanisms behind the observed atmospheric CO<sub>2</sub> decrease. The MIS 4 inception accounts for ~40 % of the total CO<sub>2</sub> decline during the last glacial cycle, which should have resulted in a cooling of the Southern Hemisphere (Menking et al., 2022; Broccoli and Manabe, 1987). In this context, the warming observed at the western margin of the South Atlantic raises a crucial question: what are the mechanisms related to this climatic exception in a period generally characterized by cold temperatures and glacial conditions?

Santos et al. (2017) and Nascimento et al. (2023) suggested that the observed warming in the western margin of the South Atlantic during MIS 4 was linked to the weakening of the Atlantic Meridional Overturning Circulation (AMOC), as it plays a major role in the interhemispheric cross-equatorial heat transport. A weakened AMOC would diminish northward heat export across the equator, accumulating warm waters on the western margin of the tropical Atlantic (Carlson et al., 2008; Chiessi et al., 2015; Santos et al., 2022). On the other hand, Venancio et al. (2018) suggested that the warming of the western margin was related to changes in the zonal component of the trade winds, as the southeast (SE) trade winds became less zonal during MIS 4. This shift was driven by changes in the intensity of the West African monsoon. The main caveat of these previous studies is that their interpretations are based on Mg/Ca results from few marine sediment cores, restricted to the western margin of the South Atlantic. Thus, there is a clear need for all available reconstructions to unravel the main mechanism underlying this warming pattern at the western South Atlantic margin during MIS 4.

Here, we present a compilation of all available Mg/Ca-based SST records from both the eastern and western margins of the South Atlantic, aiming to understand the main patterns and underlying mechanisms driving the thermal evolution during MIS 4. Despite recent progress, the mechanisms behind the anomalous warming in the western South Atlantic remain unresolved. Existing hypotheses, including weakened

AMOC or shifts in wind-driven circulation, are based on limited spatial coverage and have not yet been evaluated in a basin-wide context. By recalibrating Mg/Ca-derived SST records and comparing them with independent proxies for atmospheric CO<sub>2</sub>, ocean circulation, and orbital forcing, we aim to assess the drivers of this warming. We hypothesize that the mechanisms previously proposed to explain the MIS 4 warming become consistent with the observed pattern when SST records from both margins of the South Atlantic are integrated.

## 2. Regional setting

The uppermost circulation in the South Atlantic is composed by several currents, with emphasis on the Benguela Current System (BCS), South Equatorial Current (SEC), North Brazil Current (NBC), Brazil Current (BC) and North Equatorial Counter-Current (NECC) (Fig. 1).

The Benguela Current (BCS) is the eastern boundary current of the South Atlantic subtropical gyre. The BCS flows northwards and separates from the coast of Africa towards the northwest at ca. 30°S, being fed primarily by the South Atlantic Current (SAC), the southern current of the subtropical gyre, but also by the Agulhas Current (AC) leakage. In turn, the Benguela Upwelling System (BUS) feeds the southern branch of the SEC (Peterson and Stramma, 1991). The broad SEC flows westward to eastern South America, where it bifurcates into NBC and BC at ca. 10°S (Stramma and England, 1999). The NBC receives its major water input from the SEC and is responsible for transporting warm and saline waters to the Northern Hemisphere. It is part of the upper limb of the Atlantic Meridional Overturning Circulation (AMOC). Due to this uneven distribution of SEC waters, a considerable part of the subtropical gyre is redirected to the northern hemisphere and to the equatorial counter-currents, making BC noticeably weaker than other western boundary currents as the Gulf Stream (Peterson and Stramma, 1991).

During the austral winter, when the SEC flow is intensified by the strengthening of the wind system, the maximum transport of the NBC occurs (Johns et al., 1998). Upon reaching 6–7°N, the NBC undergoes retroflection and feeds the NECC, the main eastward surface current of the equatorial Atlantic (Philander and Pacanowski, 1986; Philander, 2001). The NECC and the NBC retroflection play a crucial role in modulating the meridional transport of heat and water across the tropical Atlantic. It carries a substantial volume of warm surface waters that accumulate in the western equatorial region, redistributing them eastward across the basin (Hénin and Hisard, 1987; Richardson et al., 1992). As such, variability in retroflection intensity can modulate the interhemispheric heat transport, potentially impacting northern hemisphere climate (Johns et al., 1998). Another important eastward flow observed is the South equatorial counter-current (SECC), which feeds the circulation in the Angola basin (Fig. 1).

The upper-level ocean circulation is mostly driven by the prevailing wind systems, notably the trade winds, an easterly wind in the tropics and subtropics. Despite their westward direction, they are related to the formation and intensification of eastward flow currents, such as the NECC (Philander and Pacanowski, 1986; Philander, 2001). The trade winds converge in the region of the Intertropical Convergence Zone (ITCZ), which shifts meridionally on a seasonal basis. During austral winter in August (Fig. 1a), the ITCZ is positioned further north, coinciding with more intense southeasterly trade winds. In contrast, during April (Fig. 1b), it is located closer to the equator, corresponding to weaker southeasterly trade winds (Philander and Pacanowski, 1986).

During austral winter, a period of maximum zonality of the SE trade winds at the equator (Fig. 2a), we observe the strengthening of these winds and the northward displacement of the ITCZ. As a result, the surface currents that flow from east to west become stronger (Philander and Pacanowski, 1986; Richardson and Reverdin, 1987). With the strengthened SEC, the SECC is enhanced and, as a consequence, the heat transport to the north of the Angola-Benguela Front (ABF) are both increased. Meanwhile, a cooling in the south of the ABF is triggered due to strengthened upwelling, which is induced by the trade winds

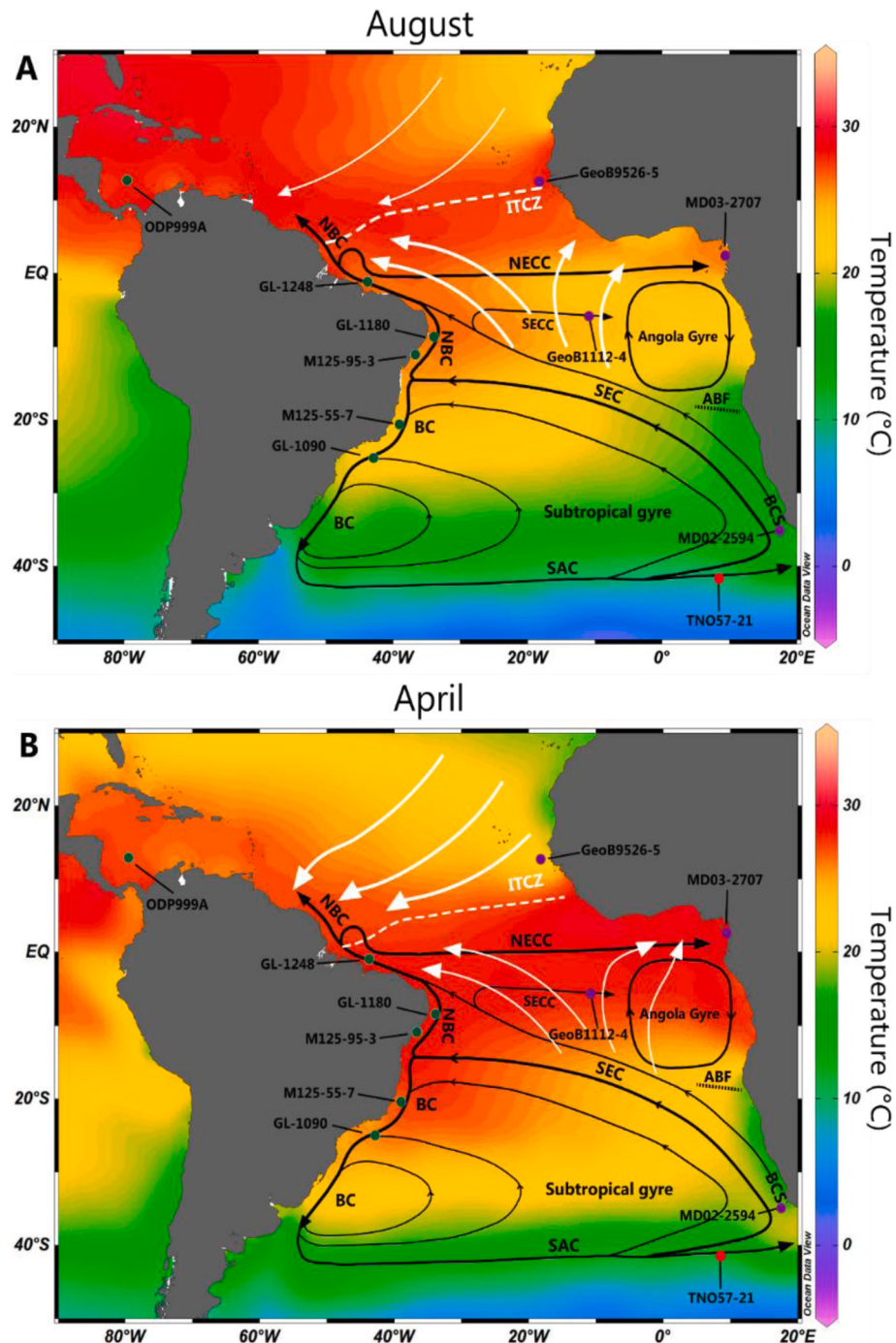


**Fig. 1.** Schematic maps showing the major uppermost currents of the South Atlantic Ocean, together with tropical atmospheric low-level circulation for August (a) and April (b). The white arrows indicate the trade winds, the black arrows indicate surface currents in the South Atlantic Ocean, and the white dotted line indicates the Intertropical Convergence Zone (ITCZ). The sediment core locations are indicated by green circles on the western margin and purple circles on the eastern margin. The surface currents shown are the Benguela Current (BCS), Brazil Current (BC), North Brazil Current (NBC), North Equatorial Counter-current (NECC), South Atlantic Current (SAC), South Equatorial Counter-current (SECC), South Equatorial Current (SEC) and the Angola-Benguela Front (ABF). Mean annual sea surface temperature is displayed in the color shading (Locarnini et al., 2019). The figure was partially generated using Ocean Data View (Schlitzer, 2023). (For interpretation of the references to color in this figure legend, the reader is referred to the Web version of this article.)

(Philander and Pacanowski, 1986; Kim et al., 2003). During the austral summer, from about February to May, there is a relaxation of the SE trade winds, proportioning a reduction in NBC flow, and the presence of the ITCZ at its southernmost position, therefore decreasing the retro-reflection in relation to the northward transport (Philander and Pacanowski, 1986).

The SE trade wind stress over the South Atlantic favors the upwelling

of cold waters and the pile-up of warm waters on the eastern and western margins, respectively (Philander and Pacanowski, 1986). Because of that, the South Atlantic thermocline is deep in the western and shallow in the eastern South Atlantic margin (Fig. 2b). Concerning the eastern margin, the region where the BCS is located is strongly influenced by the meridional component of the winds, with maximum occurring in August (Fig. 2a). Therefore, cold equatorward coastal

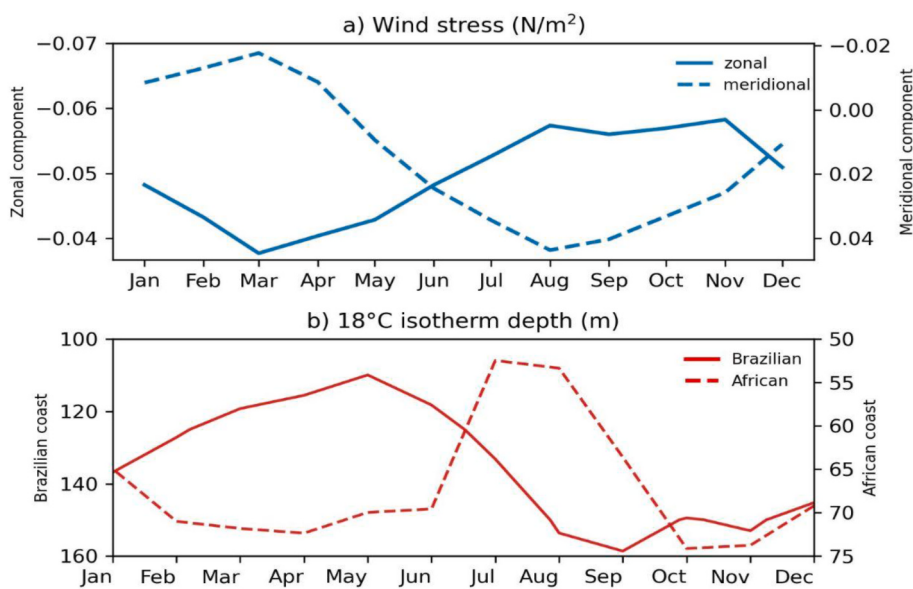


**Fig. 2.** Modern model of the trade winds in the Atlantic Ocean over the year (Josey et al., 1999). (a) The zonal and meridional components of the wind. (b) The thermocline depth at the Brazilian ( $1.5^{\circ}\text{S}$ ,  $40.5^{\circ}\text{W}$ ) and African ( $1.5^{\circ}\text{S}$ ,  $3.5^{\circ}\text{W}$ ) margins.

currents are simultaneously associated with the shoaling of the thermocline (Fig. 2b) and the enhanced upwelling along the African coast (Peterson and Stramma, 1991; Philander, 2001).

### 3. Material and methods

#### 3.1. Data compilation

Ten records of the Mg/Ca ratio analyzed in planktonic foraminifera were compiled from marine sediment cores from both margins of the South Atlantic (Table 1). The selected data covered MIS 4, but also part of MIS 5 and 3 (~75–30 ka BP). Only records with a temporal resolution better than 2 kyr were taken into account in our data compilation. Data are also provided in the supplementary material.

Mg/Ca thermometry is a well-established proxy for paleo SST. Mg and Ca are elements of long residence time in the ocean ( $10^7$  and  $10^6$  years, respectively) and their concentrations are stable over long periods (Rosenthal and Linsley, 2007). Despite the existence of other SST paleotemperature proxies, the choice of Mg/Ca can be justified by the larger number of records available on both margins of the South Atlantic compared to the more restricted alkenone-derived ( $\text{U}_{37}^k$ ) and GDGT-derived ( $\text{TEX}_{86}^H$ ) temperature records on the western South Atlantic margin (e.g., Crivellari et al., 2019; Bahr et al., 2023; Cruz et al., 2023). To ensure comparability across all records, each Mg/Ca-derived SST was generated using species-specific calibration equations from Gray and Evans (2019). Calibrations were applied according to the foraminiferal species used in each record: *Globigerinoides ruber*,

*Globigerina bulloides*, and *Trilobatus sacculifer*. For *G. ruber*, the same calibration was applied to both the white and pink morphotypes, since no significant differences in Mg/Ca temperature sensitivity between them have been reported (Richey et al., 2019).

The age models used in this compilation are based on the original chronologies provided in the respective studies (Table 1). All records are anchored by radiocarbon dating ( $^{14}\text{C}$ ), providing an independent and consistent chronological framework. Stratigraphic alignment was performed in the original works using benthic or planktonic  $\delta^{18}\text{O}$ , or elemental ratios (e.g., Ti/Ca), referenced to various global or regional stacks. Among the seven benthic  $\delta^{18}\text{O}$ -based records, two were aligned to the LR04 stack (Lisiecki and Raymo, 2005), one to the South Atlantic reference curve from Govin et al. (2014), one (GL-1090) to both LR04 and Govin et al. (2014), one to the Martinson et al. (1987) curve, and one was aligned to another sediment core. Two planktonic  $\delta^{18}\text{O}$  records were aligned to the SPECMAP stack (Basson et al., 1994a) and the  $\delta^{18}\text{O}$  record from the GISP2 ice core (Blunier and Brook, 2001), respectively. Core GL-1248 used a Ti/Ca record aligned to the  $\delta^{18}\text{O}$  record of the North Greenland Ice Core Project (NGRIP members, 2004). No additional tuning was applied. While all records are constrained by radiocarbon dating and capture well-defined climatic transitions, the use of different reference curves across sites may introduce chronological inconsistencies. Furthermore, the lack of  $\delta^{18}\text{O}$  data in some records limits the possibility of re-aligning all cores to a common reference timescale, which we acknowledge as a limitation of this compilation.

**Table 1**  
Characteristics of the compiled records.

Core ID	Latitude ( $^{\circ}\text{N}$ )	Longitude ( $^{\circ}\text{W}$ )	Water depth (m)	Species	Age model	Citation
GL-1090	-24.92	-42.51	2225	<i>G. ruber</i> (w)	$^{14}\text{C}$ , benthic $\delta^{18}\text{O}$ alignment	Santos et al. (2017)
M125-55-7	-20.36	-38.62	1960,1	<i>G. ruber</i> (p)	$^{14}\text{C}$ , benthic $\delta^{18}\text{O}$ alignment	Hou et al., 2020
M125-95-3	-10.95	-36.21	1897	<i>G. ruber</i> (p)	$^{14}\text{C}$ , benthic $\delta^{18}\text{O}$ alignment	Campos et al., 2019
GL-1180	-8.45	-33.55	1037	<i>G. ruber</i> (w)	$^{14}\text{C}$ , benthic $\delta^{18}\text{O}$ alignment	Nascimento et al. (2023)
GL-1248	-0.92	-43.40	2264	<i>G. ruber</i> (w)	$^{14}\text{C}$ , Ti/Ca alignment	Venancio et al. (2021)
ODP999A	12.74	-78.74	2828	<i>G. ruber</i> (w)	$^{14}\text{C}$ , planktonic $\delta^{18}\text{O}$ alignment	Schmidt et al. (2004)
MD02-2594	-34.71	17.34	2440	<i>G. bulloides</i>	$^{14}\text{C}$ , benthic $\delta^{18}\text{O}$ alignment	Martínez-Méndez et al., 2010
GeoB1112-4	-5.78	-10.75	3125	<i>T. sacculifer</i>	$^{14}\text{C}$ , benthic $\delta^{18}\text{O}$ alignment	Nürnberg et al. (2000)
MD03-2707	2.50	9.39	1295	<i>G. ruber</i> (p)	$^{14}\text{C}$ , planktonic $\delta^{18}\text{O}$ alignment	Weldeab et al. (2007)
GeoB9526-5	12.44	-18.057	3223	<i>G. ruber</i> (p)	$^{14}\text{C}$ , benthic $\delta^{18}\text{O}$ alignment	Zarriess et al., 2011

### 3.2. Stacks

To investigate the mean near-sea surface temperature (SST) evolution of the eastern and western South Atlantic during MIS 4, we constructed two composite records based on Mg/Ca-derived SST data from sediment cores retrieved from both continental margins (Table 1; Fig. 1). For the eastern margin, we used data from cores GeoB1112-4, GeoB9526-5, MD02-2594, and MD03-2707. For the western margin, cores GL-1090, GL-1248, GL-1180, M125-55-7, M125-95-3 and ODP Site 999A were selected. These sediment records span the MIS 4 interval, though they vary in temporal resolution. To avoid bias toward records with higher resolution, the data were interpolated to match the mean resolution of each margin, which is 0.55 kyr for the western margin and 0.69 kyr for the eastern margin.

We then utilized the Pyleoclim Python package, designed for

intuitive analysis and visualization of paleoclimate time series (Khider et al., 2022). The Mg/Ca-derived SST data were loaded as Pyleoclim series (one of the accepted input formats), and standardized to produce anomalies centered around zero, reflecting relative temperature changes. The interpolated and standardized data were aligned onto a common time axis spanning 70 to 30 ka BP using the 'common\_time' function in Pyleoclim. Finally, for each margin, we generated ensemble mean time series with associated 95 % confidence intervals and the median temperature anomaly.

### 4. Results

During MIS 4 (70 - 60 ka), an asymmetry is observed in SST evolution between the western (Fig. 3a) and eastern margins (Fig. 3b) of the South Atlantic. Several records from the western margin exhibit persistent or

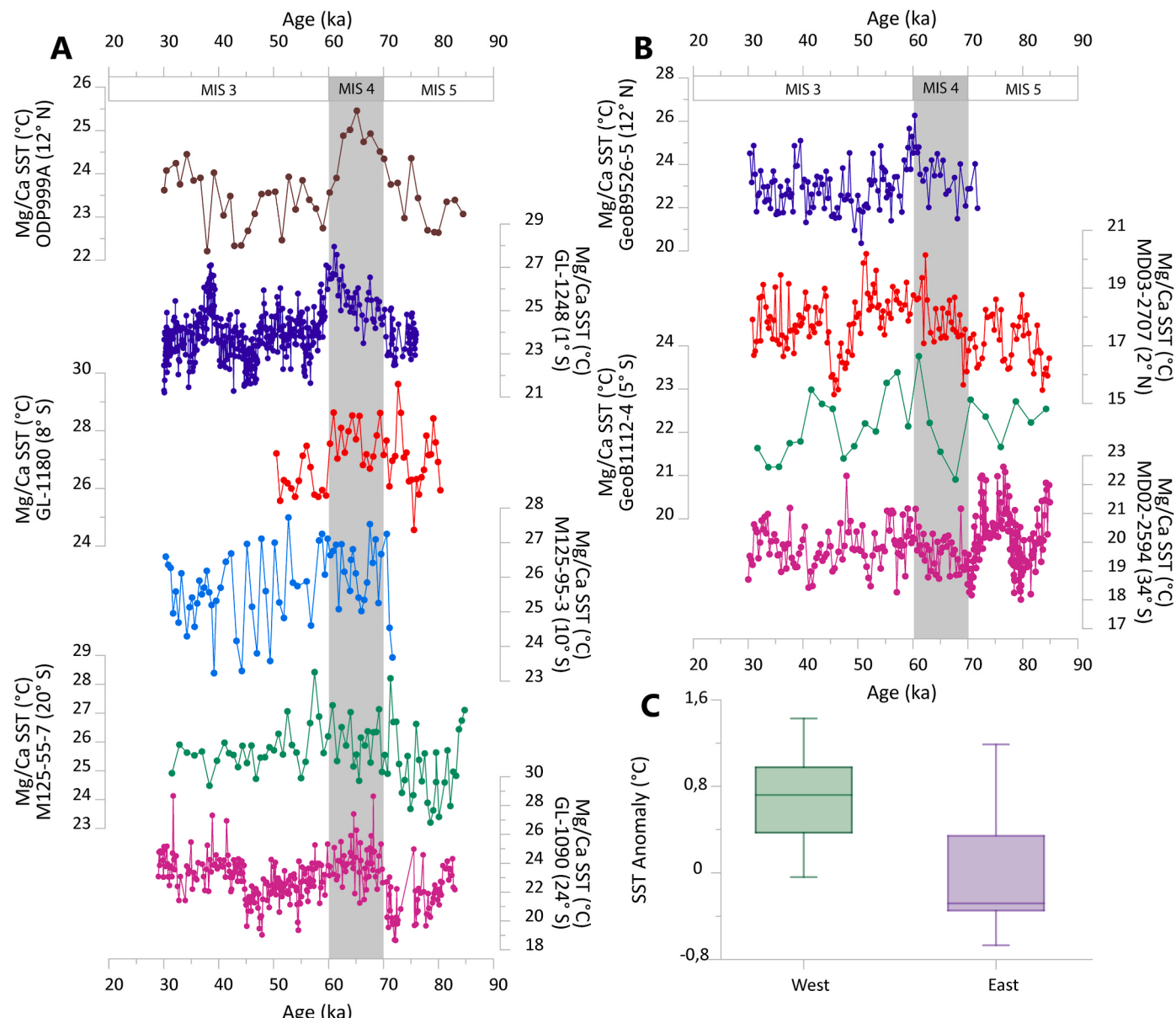


**Fig. 3.** Mg/Ca-based sea surface temperature (SST) records covering the interval from 82 to 28 ka BP from cores collected on the western (a) and eastern (b) South Atlantic margins. (a) From top to bottom: in brown, ODP999A (Schmidt et al., 2004); in purple, GL-1248 (Venancio et al., 2021); in red, GL-1180 (Nascimento et al., 2023); in light blue, M125-95-3 (Campos et al., 2019); in green, M125-55-7 (Hou et al., 2020); in pink, GL-1090 (Santos et al. 2017). (b) From top to bottom: in purple, GeoB9526-5 (Zarriess et al., 2011); in red, MD03-2707 (Weldeab et al., 2007); in green, GeoB1112-4 (Nürnberg et al., 2000); in pink, MD02-2594 (Martínez-Méndez et al., 2010). MIS are indicated in the top of the panels. (c) Box and whisker plot of the SST anomalies during Marine Isotope Stage (MIS) 4 on the western and eastern margins. (For interpretation of the references to color in this figure legend, the reader is referred to the Web version of this article.)

even increased SSTs relative to the surrounding interglacial stage, while most eastern records show a progressive cooling during this glacial stage.

**Fig. 3a** exhibits the SST records of the Mg/Ca ratio on the western margin during MIS 4, while also covering a fraction of both the MIS 5 and MIS 3 periods. The cores GL-1180 (Nascimento et al., 2023), M125-95-3 (Campos et al., 2019), M125-55-7 (Hou et al., 2020) show relatively stable or slightly increasing SSTs during MIS 4, displaying peak temperatures (Table 2) comparable to or even higher than those of MIS 3 and MIS 5. Additionally, ODP999A (Schmidt et al., 2004), GL-1248 (Venancio et al., 2021) and GL-1090 (Santos et al., 2017) display sustained elevated SSTs throughout MIS 4.

In contrast, **Fig. 3b** presents Mg/Ca-based SST records from the eastern margin of the South Atlantic, encompassing data from MIS 3, MIS 4, and MIS 5. The cores GeoB9526-5 (Zarriess et al., 2011), MD03-2707 (Weldeab et al., 2007), GeoB1112-4 (Nürnberg et al., 2000), and MD02-2594 (Martínez-Méndez et al., 2010) display a general cooling trend during MIS 4. Most of these records show minimum SSTs during the mid-stage, followed by a marked increase in SSTs toward the end of MIS 4 (~63 ka). An exception is core MD02-2594, which shows no evidence of warming and maintains low SSTs throughout the entire interval.

**Table 2** summarizes the maximum and minimum SST values for each core across MIS 3, MIS 4, and MIS 5.

**Fig. 3c** displays a statistical diagram of the SST anomaly during MIS 4, showing predominantly positive anomalies along the western margin and negative anomalies along the eastern margin. The maximum value of 1.43 °C and the minimum of -0.04 °C are observed on the western margin, with a median of 0.72 °C. On the eastern margin, the maximum SST anomaly is 1.2 °C, the minimum is -0.67 °C, and the median is -0.28 °C.

**Fig. 4** shows the SST stacks anomalies for the western (panel A) and eastern (panel B) margins of the South Atlantic between 70 and 30 ka. Anomalies were calculated relative to the mean SST of each record. In the western margin, the anomaly curve exhibits predominantly positive values throughout MIS 4. The maximum anomaly reaches approximately +1.6 °C, indicating persistent warming. In contrast, the eastern margin shows predominantly negative SST anomalies during the same interval, with values falling below -1 °C at multiple points. The onset of MIS 4 is marked by a clear cooling trend, and the anomaly remains negative until ~63 ka. Unlike the western margin, there is no indication of sustained warming during MIS 4 in the eastern composite.

**Table 2**  
Maximum and minimum sea surface temperature (SST) values (in °C) during MIS 3, MIS 4 and MIS 5.

Core ID	MIS 3		MIS 4		MIS 5	
	Max SST	Min SST	Max SST	Min SST	Max SST	Min SST
Western						
GL-1090	28.7 °C	19 °C	28.6 °C	19.6 °C	25 °C	18.6 °C
M125-55-7	28.4 °C	24.5 °C	27.3 °C	24.7 °C	28.2 °C	23.2 °C
M125-95-3	27.7 °C	23.2 °C	27.5 °C	25 °C	—	—
GL-1180	27.5 °C	25.8 °C	28.6 °C	26.7 °C	29.6 °C	24.6 °C
GL-1248	27.1 °C	21.2 °C	28 °C	23 °C	25.1 °C	22.5 °C
ODP999A	24.5 °C	22.2 °C	25.5 °C	23.6 °C	24.4 °C	22.6 °C
Eastern						
MD02-2594	22.3 °C	18.3 °C	21.2 °C	18.2 °C	22.6 °C	18 °C
GeoB1112-4	23.4 °C	21.2 °C	23.8 °C	20.9 °C	22.7 °C	21.7 °C
MD03-2707	20.2 °C	15.3 °C	20.1 °C	15.6 °C	18.8 °C	15.5 °C
GeoB9526-5	25.7 °C	20.4 °C	26.3 °C	21.5 °C	—	—

## 5. Discussion

### 5.1. Climate forcings and the thermal evolution of MIS 4

The transition from MIS 5 to 4 is characterized by a rapid global cooling and a significant drawdown in atmospheric CO<sub>2</sub> at ca. 70 ka BP (**Fig. 5d**). Barker and Diz (2014), using data from core TNO57-21, observed an abrupt cooling in the eastern South Atlantic coeval to temperature decreases in Greenland and Antarctica (**Fig. 5c** and **g**). This pattern was not typical of the bipolar seesaw, suggesting that this shift to glacial conditions occurred simultaneously in both hemispheres and roughly synchronously with the decline in CO<sub>2</sub> levels (**Fig. 5d**). The authors proposed that the ocean circulation shifted to its glacial mode due to a combination of changes in orbital configurations and the compound effects of abrupt alteration in oceanic and atmospheric circulation patterns. Specifically, the weakening of the AMOC during MIS 4, evidenced by the low values of deep North Atlantic δ<sup>13</sup>C from benthic foraminifera records (**Fig. 5e**) (Lynch-Stieglitz et al., 2014), would have enhanced the deep ocean's capacity to store CO<sub>2</sub>, leading to a reduction in atmospheric CO<sub>2</sub> levels.

Shackleton et al. (2021) reconstructed the mean ocean temperature from noble gas measurements on ancient ice samples. During the rapid decrease in atmospheric CO<sub>2</sub> (~40 ppm) from 72 to 68 ka BP, mean ocean temperature decreased by 0.90 ± 0.3 °C (**Fig. 5b**). According to the authors, ocean cooling played a significant role in controlling atmospheric CO<sub>2</sub> through the solubility pump during the transition from MIS 5 to 4. However, the long-term trend of atmospheric CO<sub>2</sub> drawdown does not correspond to the decrease in ocean temperature, suggesting that the role of the solubility pump progressively diminished as glacial inception progressed. A reorganization of the carbon cycle is required to account for the decrease in CO<sub>2</sub> levels after the early stages of the glacial inception. This reorganization can be attributed to changes in oceanic circulation as it entered its glacial mode, with a reduction in the ventilation of abyssal waters (Shackleton et al., 2021).

In this context, the biological pump may also have played a role in the significant decrease in atmospheric CO<sub>2</sub> during MIS 4. The δ<sup>13</sup>C signal can be affected by this process, as increased primary productivity enhances the uptake of nutrients and carbon, preferentially <sup>12</sup>C, leading to <sup>13</sup>C enrichment in surface waters. During the remineralization of organic matter, carbon with low <sup>13</sup>C/<sup>12</sup>C ratios is transferred to deeper water masses, thereby lowering δ<sup>13</sup>C values in the deep ocean (Oppo et al., 2015). However, multiple lines of evidence support a dominant role for reduced AMOC-driven ventilation during MIS 4. This includes the benthic δ<sup>13</sup>C gradient (Δδ<sup>13</sup>C) and trace metal records (e.g., <sup>231</sup>Pa/<sup>230</sup>Th). Variations in Δδ<sup>13</sup>C (Lisicki et al., 2008) provide valuable insights into the balance between northern- and southern-sourced water masses. A reduction in Δδ<sup>13</sup>C (**Fig. 5f**) is generally interpreted as a decline in the mixing of North Atlantic Deep Water (NADW) and Antarctic-sourced waters at intermediate depths, often associated with a weaker and/or shallower AMOC. The <sup>231</sup>Pa/<sup>230</sup>Th ratio (Böhm et al., 2015) also reflects changes in deep ocean circulation and is commonly used as a proxy for the strength of the AMOC. Higher <sup>231</sup>Pa/<sup>230</sup>Th values (**Fig. 5f**) indicate a weaker state of AMOC. Therefore, although biological processes may have contributed to CO<sub>2</sub> drawdown and δ<sup>13</sup>C changes, the observed signal during MIS 4 is most consistent with large-scale ocean circulation changes associated with a shoaled and weakened AMOC.

Our compilation of planktonic foraminiferal Mg/Ca-based SST records (**Fig. 5h** and **i**) shows a heterogeneous response concerning the eastern and western margins of the South Atlantic during the early MIS 4 (70–63 ka BP). The records from the eastern margin display a pattern similar to the synchronous inter-hemispheric cooling of Greenland and Antarctica, and are parallel to the decrease in atmospheric CO<sub>2</sub>. Instead, western margin records show the opposite trend marked by an unexpected temperature increase. In contrast, during the late MIS 4 (63–60 ka BP), SST on both margins follow the global warming pattern (**Fig. 5**).

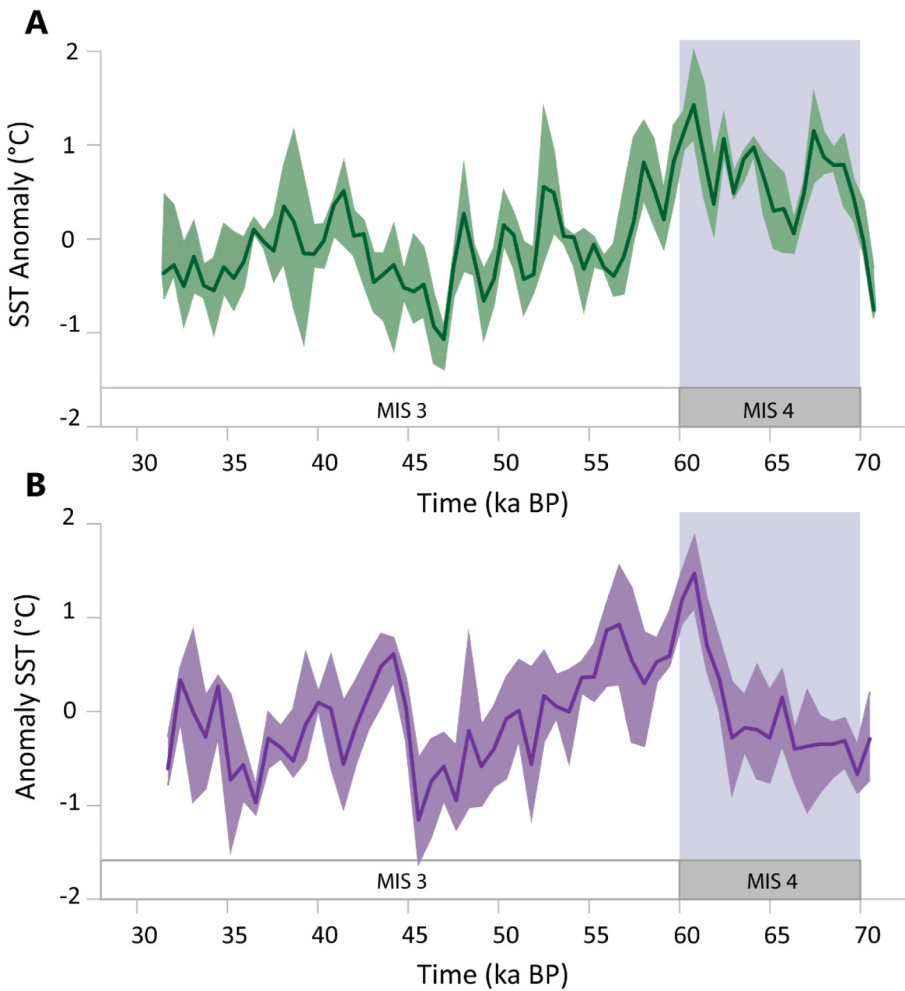


**Fig. 4.** Western (a) and eastern South Atlantic sea surface temperature (SST) stacks for Marine Isotope Stages (MIS) 4-3.

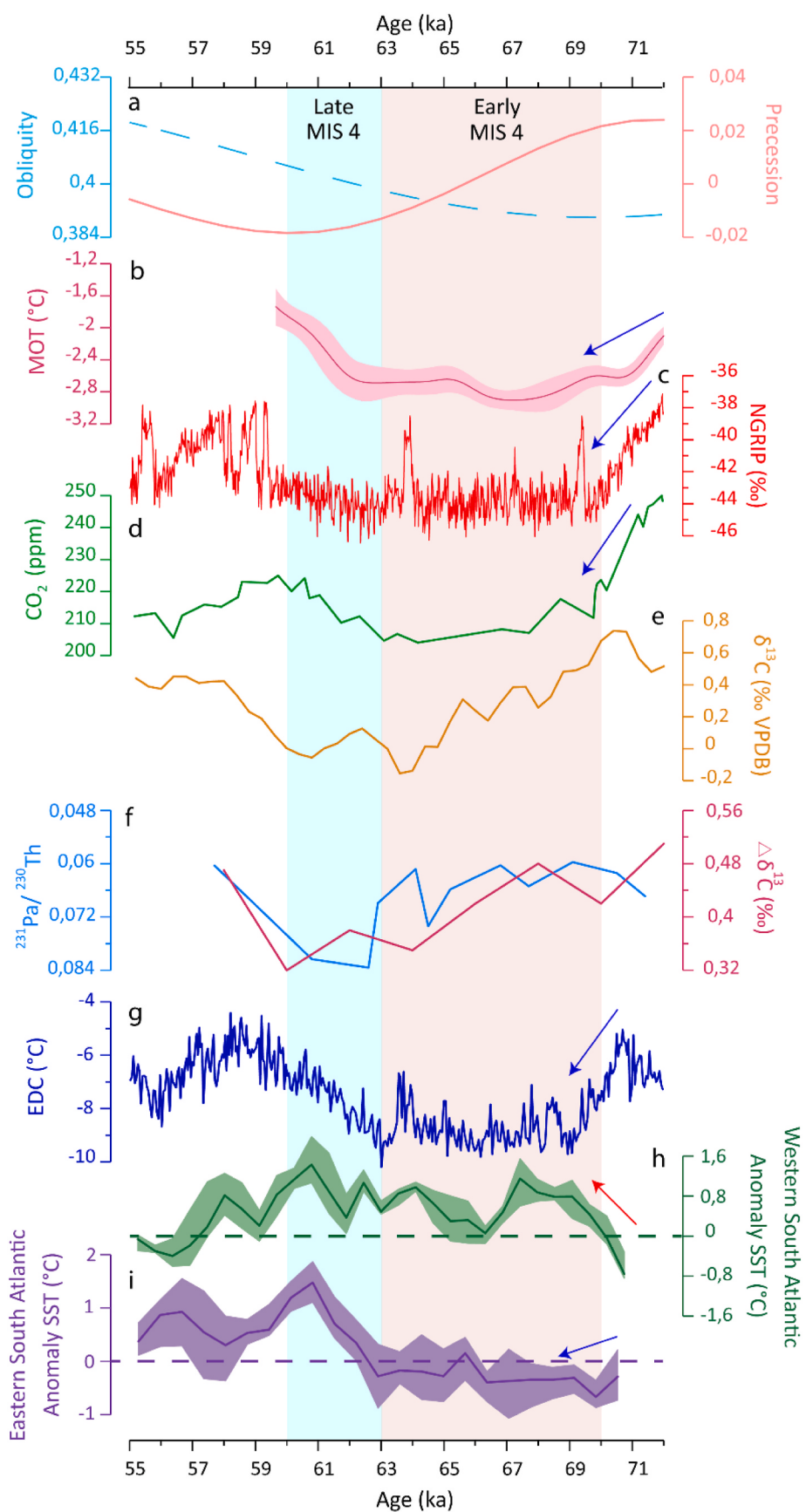
Thus, our SST stack from the western margin differs from global cooling and is at odds with expected SST variability based on changes in atmospheric CO<sub>2</sub> concentration (Shackleton et al., 2021).

The increase in SST on the western margin may be attributed to orbital parameters, particularly the low obliquity during MIS 4 (Fig. 5a). This low obliquity results in high annual mean insolation at low latitudes (Loutre et al., 2004). As highlighted by Nascimento et al. (2023), glacial warm events recorded in the western tropical Atlantic coincided with periods of elevated mean annual insolation. While such insolation likely contributed to the intensified warming, it should not be considered the dominant driver for these glacial warm events. This interpretation is reinforced by the absence of similar warming signals along the western margin of the North Atlantic, where records such as the high-resolution Mg/Ca-based SST data from core MD02-2575 (29°N, Gulf of Mexico) show no evidence of a northward propagation of these anomalies. Therefore, the warming seems to have been expressed in the western South Atlantic but not extended into the Northern Hemisphere records (Nascimento et al., 2023).

The warming on the western margin of the South Atlantic during MIS 4 has been documented in previous studies (e.g., Santos et al., 2017; Nascimento et al., 2023). The Brazil Current SST record from Santos et al. (2017) shows peak temperatures during MIS 4 that are similar to those of MIS 5, with persistently elevated temperatures throughout MIS 4. The authors attribute this warming to a complex combination of changes tied to the Antarctic Circumpolar Current, the South Atlantic subtropical gyre, mid-depth circulation, and orbital configuration. In particular, Santos et al. (2017) propose that a northward displacement

of the SEC bifurcation would divert more surface water into the BC and less into the NBC. Since the NBC is a key conduit for warm, saline waters flowing toward the Northern Hemisphere and feeding the upper limb of the AMOC, a reduction in NBC transport would diminish the interhemispheric heat and salt flux, potentially weakening the AMOC (Rodrigues et al., 2007). The NBC SST record from Nascimento et al. (2023) using Mg/Ca-based SST records from *G. ruber* (white) in core GL-1180 (8.45S, 33.55W), suggests that a long-term bipolar seesaw, driven by orbital-scale fluctuations in the AMOC, was the predominant mechanism responsible for the warming of the western South Atlantic during MIS 4. The long-term bipolar seesaw reflects a more gradual decline in AMOC strength over orbital timescales, resulting in a slower reorganization of meridional heat distribution and sustained warming in the South Atlantic without the need for abrupt circulation changes. The weakening of the AMOC would lead to a widespread warming of the South Atlantic due to the slowdown of the northward cross-equatorial warm and salty waters (Pedro et al., 2018). However, the long-term bipolar seesaw cannot fully explain the west-east South Atlantic SST contrast during MIS 4.

Thus, the proposed forcings do not fully explain the observed temperature patterns in the eastern and western margins of the South Atlantic during early MIS 4. In light of this, it becomes crucial to delve deeper into our investigations and explore new mechanisms and variables that could provide a more comprehensive and accurate understanding of the thermal evolution of the South Atlantic throughout MIS 4.



(caption on next page)

**Fig. 5.** Climate records and orbital configuration of Marine Isotope Stage (MIS) 4. (a) Obliquity (dashed blue line) and precession (solid light red line) (Berger and Loutre, 1999); (b) Mean Ocean Temperature (Shackleton et al., 2021); (c) NGRIP  $\delta^{18}\text{O}$  (Bazin et al., 2013); (d) CO<sub>2</sub> atmospheric (Bereiter et al., 2012); (e) deep North Atlantic  $\delta^{13}\text{C}$  (Lynch-Stieglitz et al., 2014); (f)  $^{231}\text{Pa}/^{230}\text{Th}$  ratio in solid blue line (Böhm et al., 2015) and benthic  $\delta^{13}\text{C}$  gradient in solid wine line (Lisicki et al., 2008); (g) EPICA Dome C (EDC) temperature anomalies relative to the average of the last 1000 years (Jouzel and Masson-Delmotte, 2007); (h) western South Atlantic SST stack (this study); (i) eastern South Atlantic SST stack (this study). (For interpretation of the references to color in this figure legend, the reader is referred to the Web version of this article.)

## 5.2. Disentangling the mechanisms responsible for the South Atlantic thermal evolution during MIS 4

The trade winds, known for their predominant east-west direction, significantly influence ocean circulation in the tropics and subtropics. Ocean surface circulation is inherently affected by the strength of these

winds, playing a crucial role in thermal variability, heat distribution, and specific weather patterns of the Atlantic Ocean (Merle, 1980; Carton and Zhou, 1997). During austral winter, the SE trade winds are enhanced due to the temperature contrast between the tropical and subtropical latitudes of the South Atlantic (Wolff et al., 1999). From a dynamical standpoint, this strengthening is also supported by the

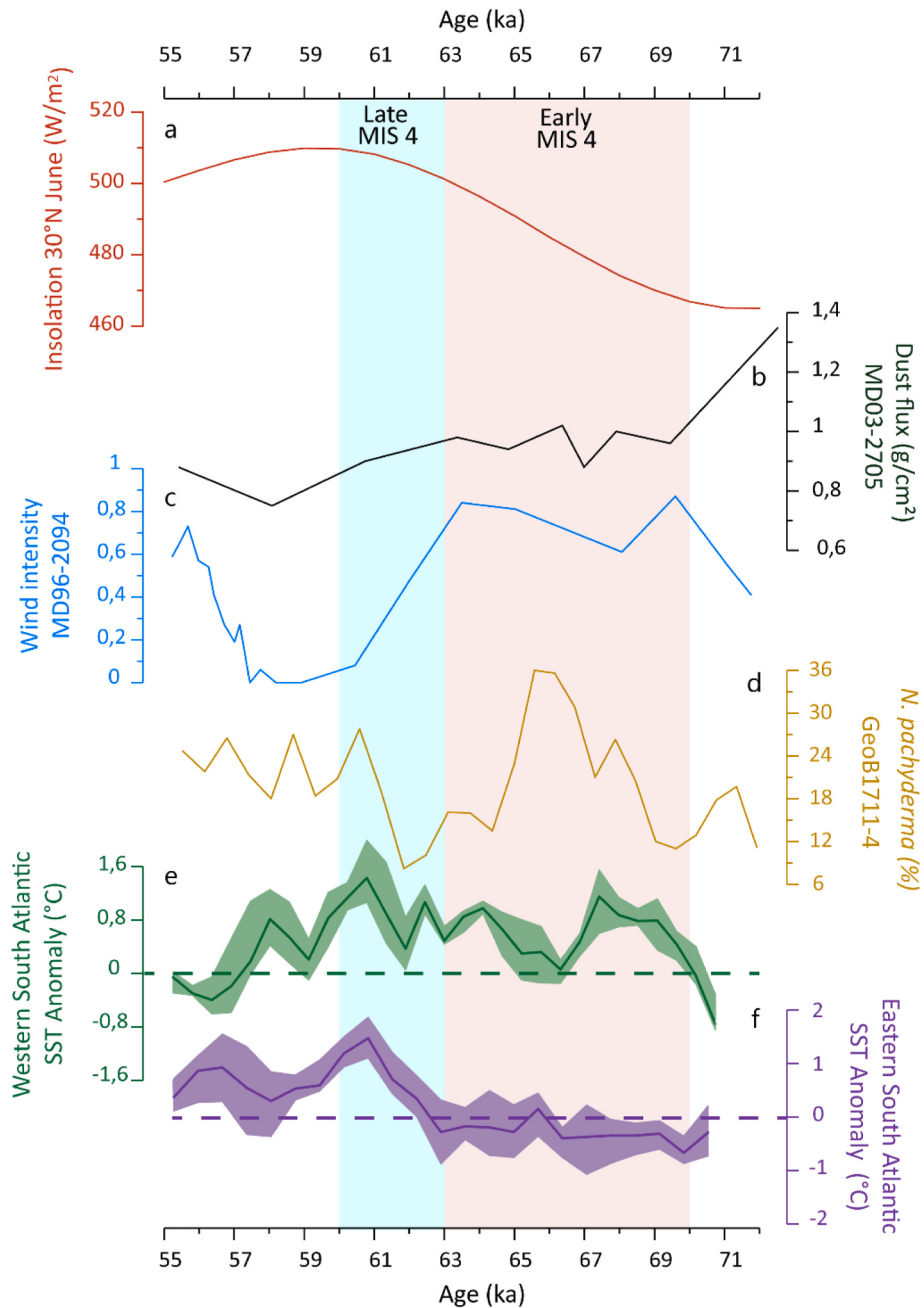


**Fig. 6.** Comparison of Atlantic Ocean trade wind proxies with South Atlantic sea surface temperature (SST) stacks during Marine Isotope Stage (MIS) 4. (a) Mid-June 30°N insolation (Berger and Loutre, 1999); (b) dust flux from marine sediment core MD03-2705 (18.08°N, 21.15°W) (Skoneczny et al., 2019) (c) Wind Intensity from core MD96-2094 (20°N, 9.26°E) (Stuut et al., 2002); (d) relative abundance of *Neogloboquadrina pachyderma* from core GeoB1711-4 (23.31°S, 12.37°E) (Little et al., 1997); (e) western South Atlantic SST stack (this study); (f) eastern South Atlantic SST stack (this study).

intensification of the Hadley circulation in the Southern Hemisphere during colder periods. As the subtropics cool, the meridional temperature gradient increases, reinforcing the pressure difference between the equator and higher latitudes. This, in turn, enhances the strength of the descending branch of the Hadley cell and intensifies the SE trade winds (McGee et al., 2018). As the SE trade winds intensify, warm water masses are propelled westward, primarily due to enhanced westward currents, particularly the SEC (Molinari, 1983; Johns et al., 1998). As warm waters accumulate on the western margin, an asymmetry in the east-west thermocline emerges, resulting in deepening on the western margin and shoaling on the eastern margin (Fig. 2) (Merle, 1980; Philander and Pacanowski, 1986). Consequently, a contrast in SST between the eastern and western margins emerges due to the intensified SE trade winds.

During glacial periods, the Antarctic polar front, the Subantarctic front, and the Subtropical front in the South Atlantic shift towards the equator, amplifying the meridional pressure gradient and leading to the intensification of the SE trade winds (Stuut et al., 2002; Pinho et al., 2025). Through an analysis of grain-size distribution in core MD96-2094 (retrieved off southwestern Africa) spanning the last 300 ka BP, Stuut et al. (2002) observed an increase in trade winds strength during glacial periods compared to interglacial periods (Fig. 6c), including the early MIS 4. Little et al. (1997) proposed that the intensified trade winds are responsible for the increased upwelling intensity in the Benguela region during early MIS 4. This enhanced upwelling is indicated by the increase in the abundance of *Neogloboquadrina pachyderma sinistral* (Fig. 6d), a near-surface cold-water planktonic foraminifera species, in core GeoB1711-4. Analyzing the same marine sediment core, Shi et al. (2001) also reported a trade wind strengthening during glacial periods based on the increased influx of anemophilous pollen.

When boreal summer encompasses perihelion, the west African monsoon intensifies, reducing the zonal component of the trade winds while amplifying their meridional component, with the opposite occurring when boreal winter encompasses perihelion (McIntyre et al., 1989; Molino and McIntyre, 1990). The timing of perihelion is primarily controlled by orbital precession (Fig. 5a), which dictates whether perihelion falls in summer or winter. This modulation of wind zonality by the monsoon is attributed to changes in convergence over northern Africa's landmass (McIntyre et al., 1989). Therefore, during the first half of MIS 4, the low boreal summer insolation in the Northern Hemisphere (Fig. 6a) resulted in a weakened west African monsoon and was responsible for an increase in the zonality of the SE trade winds.

Thus, for the early MIS 4, an increase in westward flow by the SEC, driven by the intensification of the SE trade winds, a piled-up warm waters in the western South Atlantic, explaining the positive temperature anomaly in the western South Atlantic stack (Fig. 6e). In the eastern South Atlantic, the intensified zonal component of the SE trade winds drives surface waters away from the coast, leading to offshore surface drift and coastal upwelling of cold and nutrient-rich waters (Peterson and Stramma, 1991). The upwelling phenomenon notably intensifies during the austral spring a period in which, as depicted in Fig. 2b, the zonal component of the wind enhances (Peterson and Stramma, 1991; Carton and Zhou, 1997). This is also supported by Molino and McIntyre (1990), who observed changes in the intensity of upwelling on the eastern equatorial margin by measuring the depth of the nutricline based on the abundance of *Florisphaera profunda*. The low abundance of *F. profunda* on the onset MIS 4 suggests a shallow nutricline, indicative of lower temperatures due to enhanced upwelling on the eastern South Atlantic margin. This explains the negative SST anomaly in the eastern South Atlantic stack during the early MIS 4 (Fig. 6f).

This mechanism is in line with studies that report a relatively weak west African monsoon, or more arid conditions over northern Africa (Fig. 6b), especially during early MIS 4 (Pokras and Mix, 1987; Weldeab et al., 2007; Skonieczny et al., 2019). In addition, it is consistent with the deepening of the thermocline along the western South Atlantic margin, as noted by Hou et al. (2020) for some glacial periods. In that study, they

reported an anomalous warming on the western margin during MIS 6 (191–130 ka BP), potentially linked to the increased strength in the SE trade winds.

Although the early MIS 4 is characterized by a relatively more active AMOC and intensified southeast trade winds compared to its later phase, which could imply enhanced NBC transport and increased northward heat export, potentially contributing to cooling on the western margin, the outcome depends critically on the position of the SEC bifurcation. As discussed by Santos et al. (2017), in the event of a northward shift in the bifurcation, a greater proportion of the SEC is redirected into the BC, whilst the contribution to the NBC is reduced. This redistribution weakens the interhemispheric heat transport despite overall stronger circulation. Model results from Rodrigues et al. (2007) show that the latitude of the bifurcation is highly sensitive to variations in local wind stress curl, which are in turn linked to seasonal shifts in the ITCZ. Proxy-based reconstructions of tropical precipitation suggest that the ITCZ remained in a relatively southern position between 70 and 60 ka (Deplazes et al., 2013; Wang et al., 2004). This setting would have promoted a more northerly location of the SEC bifurcation. Combined with a northward expansion of the subtropical gyre and the Antarctic Circumpolar Current system, this configuration would favor a stronger BC and a reduced NBC, thereby diminishing heat transfer to the Northern Hemisphere even during periods of active overturning. The ITCZ reached its southernmost position around ~64 ka (Deplazes et al., 2013; Wang et al., 2004), coinciding with the maximum AMOC weakening (Fig. 5e and f). As a result, heat would tend to accumulate in the western South Atlantic, contributing to the sustained warming observed in this region during early MIS 4.

For the late MIS 4, Northern Hemisphere summer insolation is high (Fig. 6a), which results in a strong west African monsoon and a decrease in the zonal component of the SE trade winds, promoting a reduction in the SEC transport and in the advection of warm waters towards the western South Atlantic. However, we still observe positive temperature anomalies during the late MIS 4 in the western South Atlantic margin (Fig. 6e). At the same time, the eastern margin also shows positive anomalies (Fig. 6f). These observations require an additional mechanism capable of sustaining the warming in the western margin and inducing warming in the eastern margin during the late MIS 4. The millennial-scale bipolar seesaw mechanism is typically associated with an anti-phase temperature evolution between Greenland and Antarctica (Stocker and Johnsen, 2003). As illustrated in Fig. 5c and g, a discernible warming of Antarctica is observed in comparison to Greenland. During this interval, a reduction in AMOC strength is observed (Fig. 5e and f) probably due to enhanced meltwater influx into the Northern Hemisphere (Adkins, 2013). Indeed, the so-called "late MIS 4" in this study is equivalent to Heinrich Stadial 6 (HS6), which is characterized by a weak AMOC (Fig. 5e and f), an increase in atmospheric CO<sub>2</sub> (Fig. 5d) and in global temperatures (Fig. 5b and g). Thus, the temperature increases over the South Atlantic is linked to the bipolar seesaw mechanism, which served as the primary driver of warming during this period. This pattern is evident in our stacks, along with a corresponding temperature decrease over the North Atlantic. Nonetheless, this mechanism can only account for the final phase of MIS 4.

Summarizing, we propose that the SST contrast between the eastern and western margins of the South Atlantic during early MIS 4 (Fig. 7a) was primarily driven by a sequence of processes initiated by reduced summer insolation in the Northern Hemisphere. This insolation minimum weakened the West African monsoon, which in turn increased the zonal component of the SE trade winds. The resulting wind pattern intensified the SEC, enhancing westward surface water transport and favoring heat accumulation along the western margin. At the same time, the strong SE trade winds intensified upwelling along the eastern margin, contributing to SST cooling offshore Africa. In contrast, during late MIS 4/HS6 (Fig. 7b), SST evolution on both margins became more synchronous. This pattern reflects the combined influence of a weakened AMOC, a reduction in trade wind strength, and a gradual rise in

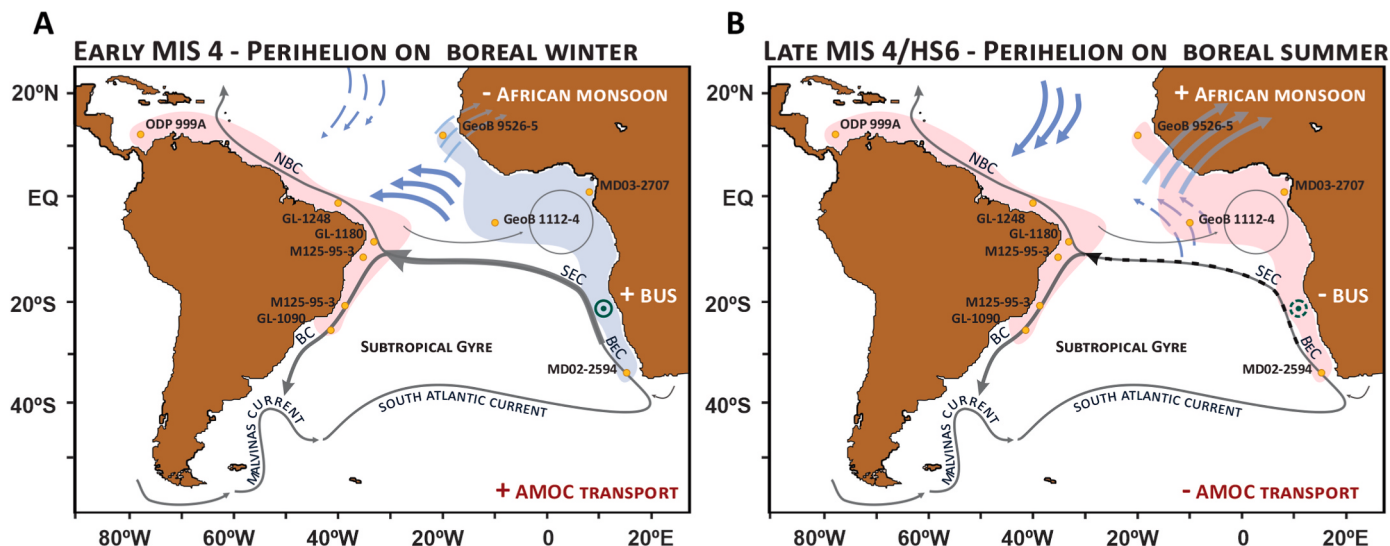


**Fig. 7.** Schematic illustration of the mechanisms responsible for the thermal evolution of the South Atlantic during the early (a) and late (b) Marine Isotope Stage (MIS) 4, including the intensity and zonality of the trade winds (blue arrows), intensity of surface ocean circulation (grey arrows), and sea surface temperature. The yellow dots mark the position of the cores used in this study. (For interpretation of the references to color in this figure legend, the reader is referred to the Web version of this article.)

atmospheric CO<sub>2</sub> concentrations, factors that promoted basin-wide warming and reduced the thermal asymmetry observed earlier in MIS 4.

## 6. Conclusions

According to our compilation, SST on the eastern margin of the South Atlantic followed the global cooling trend during the transition MIS 5-4, which is in agreement with the temperature trends recorded in Greenland and Antarctica ice cores, as well with the decrease in atmospheric CO<sub>2</sub>. In contrast, the western South Atlantic experienced an unexpected warming during the early MIS 4. The warming on the western margin cannot be attributed to the decrease in atmospheric CO<sub>2</sub>. Also, it is unlikely that a weakening of the AMOC alone during early MIS 4 would produce the SST contrast observed on the eastern and western South Atlantic margins. We propose that the thermal contrast observed in the first half of MIS 4 was caused by changes in the SE trade winds. During the onset of MIS 4, summer insolation minima in the Northern Hemisphere led to an increase in the zonal component of the SE trade winds and a weak west African monsoon. This, in turn, enhanced the SEC, transporting warm waters to the western South Atlantic margin. The intense and more zonal SE trade winds caused an increase in upwelling in the eastern South Atlantic margin, resulting in lower temperatures offshore Africa. These findings suggest that the trade wind system played a more prominent role in upper-ocean circulation and, ultimately, in the thermal evolution of the South Atlantic during the early MIS 4 than previously reported. For the late MIS 4/HS6 was characterized by a synchronous thermal evolution between the western and eastern margins, explained by the weakened AMOC and the increase of atmospheric CO<sub>2</sub> concentration. The combined effect of these factors resulted in a synchronous temperature increase in the western and eastern margins of the South Atlantic.

## Credit author statement

**Pedrazzi-Chacon, A.B.:** Conceptualization, Writing – original draft.  
**Venancio, I.M.:** Conceptualization, Supervision, Writing – review & editing.  
**Santos, T.P.; Ballalai, J.M.; Nascimento, R.A.; Campos, M.C., Chiessi, C.M.; Shimizu, M.H.; Albuquerque, A.L.S.:** Writing – review & editing.

## Declaration of competing interest

The authors declare that they have no known competing financial interests or personal relationships that could have appeared to influence the work reported in this paper.

## Acknowledgments

J.M. Ballalai acknowledges the financial support from FAPERJ - Fundação Carlos Chagas Filho de Amparo à Pesquisa do Estado do Rio de Janeiro (grant 260003/001327/2025). M.C.C. acknowledges the financial support from FAPESP (grants 2022/06452-0, 2023/05764-0). C.M. Chiessi acknowledges the financial support from FAPESP (grants 2018/15123-4 and 2019/24349-9), CNPq (grant 312458/2020-7) and CAPES-COFECUB (grants 8881.712022/2022-1 and 49558SM). I.M.V acknowledges the financial support from FAPERJ (SEI-260003/000677/2023, JCNE Grant 200.120/2023-281226) and CNPq (403894/2023-9). T.P.S. thanks the Programa de Apoio a Novos Docentes (Processo 22.1.09345.01.2) of the University of São Paulo. A.B.P.C thanks CAPES (grants 88887.968136/2024-00 and 88887.674064/2022-00).

## Appendix A. Supplementary data

Supplementary data to this article can be found online at <https://doi.org/10.1016/j.quascirev.2025.109613>.

## Data availability

A link to the data and/or code is provided as part of this submission.

## References

- Adkins, J.F., 2013. The role of deep ocean circulation in setting glacial climates. *Paleoceanography* 28, 539–561. <https://doi.org/10.1002/palo.20046>.
- Bahr, A., Jaeschke, A., Hou, A., Meier, K., Chiessi, C.M., Albuquerque, A.L.S., Rethemeyer, J., Friedrich, O., 2023. A Comparison Study of Mg/Ca-, Alkenone-, and TEX 86 -Derived Temperatures for the Brazilian Margin, vol. 38. *Paleoceanog and Paleoclimatol*, e2023PA004618. <https://doi.org/10.1029/2023PA004618>.
- Barker, S., Diz, P., 2014. Timing of the descent into the last ice age determined by the bipolar seesaw. *Paleoceanography* 29, 489–507. <https://doi.org/10.1002/2014PA002623>.
- Bassinot, F.C., Labeyrie, L.D., Vincent, E., Quidelleur, X., Shackleton, N.J., Lancelot, Y., 1994. The astronomical theory of climate and the age of the Brunhes-Matuyama

- magnetic reversal. *Earth Planet Sci. Lett.* 126, 91–108. [https://doi.org/10.1016/0018-821X\(94\)90244-5](https://doi.org/10.1016/0018-821X(94)90244-5).
- Bazin, L., Landais, A., Lemieux-Dudon, B., Toyé Mahamadou Kele, H., Veres, D., Parrenin, F., Martinerie, P., Ritz, C., Capron, E., Lipenkov, V.Y., Loutre, M.-F., Raynaud, D., Vinther, B.M., Svensson, A.M., Rasmussen, S.O., Severi, M., Blunier, T., Leuenberger, M.C., Fischer, H., Masson-Delmotte, V., Chappellaz, J.A., Wolff, E.W., 2013. delta 18O measured on ice core NGRIP on AICC2012 chronology. <https://doi.org/10.1594/PANGAEA.824889>.
- Bereiter, B., Lüthi, D., Siegrist, M., Schüpbach, S., Stocker, T.F., Fischer, H., 2012. Mode change of millennial CO<sub>2</sub> variability during the last glacial cycle associated with a bipolar marine carbon seesaw. *Proc. Natl. Acad. Sci. USA* 109, 9755–9760. <https://doi.org/10.1073/pnas.1204069109>.
- Berger, A., Loutre, M.F., Parameters of the Earths orbit for the last 5 Million years in 1 kyr resolution. <https://doi.org/10.1594/PANGAEA.5604>.
- Blunier, T., Brook, E.J., 2001. Timing of millennial-scale climate change in Antarctica and Greenland during the last glacial period. *Science* 291, 109–112. <https://doi.org/10.1126/science.291.5501.109>.
- Bohm, E., Lippold, J., Gutjahr, M., Frank, M., Blaser, P., Antz, B., Fohlmeister, J., Frank, N., Andersen, M.B., Deininger, M., 2015. Strong and deep Atlantic meridional overturning circulation during the last glacial cycle. *Nature* 517, 73–76. <https://doi.org/10.1038/nature14059>.
- Broccoli, A.J., Manabe, S., 1987. The influence of continental ice, atmospheric CO<sub>2</sub>, and land albedo on the climate of the last glacial maximum. *Climate Dynamics* 1, 87–99. <https://doi.org/10.1007/BF01054478>.
- Campos, M.C., Chiessi, C.M., Prange, M., Mulitza, S., Kuhnert, H., Paul, A., Venancio, I.M., Albuquerque, A.L.S., Cruz, F.W., Bahr, A., 2019. A new mechanism for millennial scale positive precipitation anomalies over tropical South America. *Quat. Sci. Rev.* 225, 105990. <https://doi.org/10.1016/j.quascirev.2019.105990>.
- Carlson, A.E., Oppo, D.W., Came, R.E., LeGrande, A.N., Keigwin, L.D., Curry, W.B., 2008. Subtropical Atlantic salinity variability and Atlantic meridional circulation during the last deglaciation. *Geol* 36, 991. <https://doi.org/10.1130/G25080A.1>.
- Carton, J.A., Zhou, Z., 1997. Annual cycle of sea surface temperature in the tropical Atlantic Ocean. *J. Geophys. Res.* 102, 27813–27824. <https://doi.org/10.1029/97JC02197>.
- Chiessi, C.M., Mulitza, S., Mollenhauer, G., Silva, J.B., Groeneveld, J., Prange, M., 2015. Thermal evolution of the western South Atlantic and the adjacent continent during termination 1. *Clim. Past* 11, 915–929. <https://doi.org/10.5194/cp-11-915-2015>.
- Crivellari, S., Chiessi, C.M., Kuhnert, H., Häggi, C., Mollenhauer, G., Hefter, J., Portilho-Ramos, R., Schefuß, E., Mulitza, S., 2019. Thermal response of the western tropical Atlantic to slowdown of the Atlantic Meridional overturning circulation. *Earth Planet Sci. Lett.* 519, 120–129. <https://doi.org/10.1016/j.epsl.2019.05.006>.
- Cruz, J.F., Boulaabassi, I., Huguet, A., Rodrigues, A.M.S., Santos, T.P., Venancio, I.M., Lessa, D., Sobrinho, R.L., Nascimento, R.A., Bernardes, M.C., 2023. Multiproxy reconstruction of late quaternary upper ocean temperature in the subtropical southwestern Atlantic. *Quat. Sci. Rev.* 307, 108044. <https://doi.org/10.1016/j.quascirev.2023.108044>.
- Cutler, K.B., Edwards, R.L., Taylor, F.W., Cheng, H., Adkins, J., Gallup, C.D., Cutler, P.M., Burr, G.S., Bloom, A.L., 2003. Rapid sea-level fall and deep-ocean temperature change since the last interglacial period. *Earth Planet Sci. Lett.* 206, 253–271. [https://doi.org/10.1016/S0012-821X\(02\)01107-X](https://doi.org/10.1016/S0012-821X(02)01107-X).
- Deplazes, G., Lückge, A., Peterson, L.C., Timmermann, A., Hamann, Y., Hughen, K.A., Röhl, U., Laj, C., Cane, M.A., Sigman, D.M., Haug, G.H., 2013. Links between tropical rainfall and North Atlantic climate during the last glacial period. *Nat. Geosci.* 6, 213–217. <https://doi.org/10.1038/ngeo1712>.
- Doney, S.C., Ruckelshaus, M., Emmett Duffy, J., Barry, J.P., Chan, F., English, C.A., Galindo, H.M., Grebmeier, J.M., Hollowed, A.B., Knowlton, N., Polovina, J., Rabalais, N.N., Sydeman, W.J., Talley, L.D., 2012. Climate change impacts on marine ecosystems. *Ann. Rev. Mar. Sci.* 4, 11–37. <https://doi.org/10.1146/annurev-marine-041911-111611>.
- Doughty, A.M., Kaplan, M.R., Peltier, C., Barker, S., 2021. A maximum in global glacier extent during MIS 4. *Quat. Sci. Rev.* 261, 106948. <https://doi.org/10.1016/j.quascirev.2021.106948>.
- Gavin, A., Chiessi, C.M., Zabel, M., Sawakuchi, A.O., Heslop, D., Hörner, T., Zhang, Y., Mulitza, S., 2014. Terrigenous input off northern South America driven by changes in Amazonian climate and the North Brazil Current retroflection during the last 250 ka. *Clim. Past* 10, 843–862. <https://doi.org/10.5194/cp-10-843-2014>.
- Gray, W.R., Evans, D., 2019. Nonthermal influences on Mg/Ca in planktonic foraminifera: a review of culture studies and application to the last glacial maximum. *Paleoceanogr. Paleoclimatol.* 34, 306–315. <https://doi.org/10.1029/2018PA003517>.
- Hénin, C., Hisard, P., 1987. The north equatorial countercurrent observed during the programme français ocean climat dans l'atlantique equatorial experiment in the Atlantic Ocean, July 1982 to August 1984. *J. Geophys. Res.* 92, 3751–3758. <https://doi.org/10.1029/JC092iC04p03751>.
- Hou, A., Bahr, A., Schmidt, S., Strelb, C., Albuquerque, A.L., Chiessi, C.M., Friedrich, O., 2020. Forcing of western tropical South Atlantic sea surface temperature across three glacial-interglacial cycles. *Global Planet. Change* 188, 103150. <https://doi.org/10.1016/j.gloplacha.2020.103150>.
- Johns, W.E., Lee, T.N., Beardsley, R.C., Candela, J., Limeburner, R., Castro, B., 1998. Annual cycle and variability of the North Brazil Current. *J. Phys. Oceanogr.* 28, 103–128. [https://doi.org/10.1175/1520-0485\(1998\)028<0103:ACAVOT>2.0.CO;2](https://doi.org/10.1175/1520-0485(1998)028<0103:ACAVOT>2.0.CO;2).
- Josey, S.A., Kent, E.C., Taylor, P.K., 1999. New insights into the ocean heat budget closure problem from analysis of the SOC air-sea flux climatology. *J. Clim.* 12, 2856–2880. [https://doi.org/10.1175/1520-0442\(1999\)012<2856:NIOHTO>2.0.CO;2](https://doi.org/10.1175/1520-0442(1999)012<2856:NIOHTO>2.0.CO;2).
- Jouzel, J., Masson-Delmotte, V., 2007. EPICA Dome C ice core 800KYr deuterium data and temperature estimates. <https://doi.org/10.1594/PANGAEA.683655>.
- Khider, D., Emile-Geay, J., Zhu, F., James, A., Landers, J., Ratnakar, V., Gil, Y., 2022. Pyeoclim: Paleoclimate timeseries analysis and visualization with python. *Paleoceanogr. Paleoclimatol.* 37, e2022PA004509. <https://doi.org/10.1029/2022PA004509>.
- Kim, J.-H., Schneider, R.R., Multizta, S., Müller, P.J., 2003. Reconstruction of SE trade-wind intensity based on sea-surface temperature gradients in the Southeast Atlantic over the last 25 kyr: reconstruction of SE trade wind. *Geophys. Res. Lett.* 30. <https://doi.org/10.1029/2003GL017557>.
- Kohfeld, K.E., Chase, Z., 2017. Temporal evolution of mechanisms controlling ocean carbon uptake during the last glacial cycle. *Earth Planet Sci. Lett.* 472, 206–215. <https://doi.org/10.1016/j.epsl.2017.05.015>.
- Lisiecki, L.E., Raymo, M.E., 2005. A pliocene-pleistocene stack of 57 globally distributed benthic δ<sup>18</sup>O records. *Paleoceanography* 20. <https://doi.org/10.1029/2004PA001071>.
- Lisiecki, L.E., Raymo, M.E., Curry, W.B., 2008. Atlantic overturning responses to late Pleistocene climate forcings. *Nature* 456, 85–88. <https://doi.org/10.1038/nature07425>.
- Little, M.G., Schneider, R.R., Kroon, D., Price, B., Bickert, T., Wefer, G., 1997. Rapid paleoceanographic changes in the Benguela upwelling system for the last 160,000 years as indicated by abundances of planktonic Foraminifera. *Palaeogeogr. Palaeoclimatol. Palaeoecol.* 130, 135–161. [https://doi.org/10.1016/S0031-0182\(96\)00136-8](https://doi.org/10.1016/S0031-0182(96)00136-8).
- Locarnini, R.A., Mishonov, A.V., Baranova, O.K., Boyer, T.P., Zweng, M.M., Garcia, H.E., Reagan, J.R., Seidov, D., Weathers, K.W., Paver, C.R., Smolyar, I.V., 2019. World Ocean atlas 2018, volume 1: temperature. A. Mishonov, technical editor. NOAA Atlas NESDIS 81, 52.
- Loutre, M.-F., Paillard, D., Vimeux, F., Cortijo, E., 2004. Does mean annual insolation have the potential to change the climate? *Earth Planet Sci. Lett.* 221, 1–14. [https://doi.org/10.1016/S0012-821X\(04\)00108-6](https://doi.org/10.1016/S0012-821X(04)00108-6).
- Lynch-Stieglitz, J., Schmidt, M.W., Gene Henry, L., Curry, W.B., Skinner, L.C., Mulitza, S., Zhang, R., Chang, P., 2014. Muted change in Atlantic overturning circulation over some glacial-aged Heinrich events. *Nat. Geosci.* 7, 144–150. <https://doi.org/10.1038/ngeo2045>.
- Martínez-Méndez, G., Zahn, R., Hall, I.R., Peeters, F.J.C., Pena, L.D., Cacho, I., Negre, C., 2010. Multicentennial Resolution Proxy Records from Splicings of MD96-2080 and MD02-2594, Agulhas Bank Splice (ABS). <https://doi.org/10.1594/PANGAEA.810716>.
- Martinson, D.G., Pisias, N.G., Hays, J.D., Imbrie, J., Moore, T.C., Shackleton, N.J., 1987. Age dating and the orbital theory of the ice ages: development of a high-resolution 0 to 300,000-Year chronostratigraphy. *Quat. Res.* 27, 1–29. [https://doi.org/10.1016/0033-5894\(87\)90046-9](https://doi.org/10.1016/0033-5894(87)90046-9).
- McIntyre, A., Ruddiman, W.F., Karlin, K., Mix, A.C., 1989. Surface water response of the equatorial Atlantic Ocean to orbital forcing. *Paleoceanography* 4, 19–55. <https://doi.org/10.1029/PA004i001p00019>.
- McGee, D., Moreno-Chamarro, E., Green, B., Marshall, J., Galbraith, E., Bradtmiller, L., 2018. Hemispherically asymmetric trade wind changes as signatures of past ITCZ shifts. *Quat. Sci. Rev.* 180, 214–228. <https://doi.org/10.1016/j.jqr.2017.11.020>.
- Menking, J.A., Shackleton, S.A., Bauska, T.K., Buffen, A.M., Brook, E.J., Barker, S., Severinghaus, J.P., Dyonisius, M.N., Petrenko, V.V., 2022. Multiple carbon cycle mechanisms associated with the glaciation of marine isotope stage 4. *Nat. Commun.* 13, 5443. <https://doi.org/10.1038/s41467-022-33166-3>.
- Merle, J., 1980. Seasonal heat budget in the equatorial Atlantic Ocean. *J. Phys. Oceanogr.* 10 (3), 464–469. [https://doi.org/10.1175/1520-0485\(1980\)010<0464:SHBTE>2.0.co;2](https://doi.org/10.1175/1520-0485(1980)010<0464:SHBTE>2.0.co;2).
- Molfino, B., McIntyre, A., 1990. Precessional forcing of nutricline dynamics in the equatorial Atlantic. *Science* 249, 766–769. <https://doi.org/10.1126/science.249.4970.766>.
- Molinari, R.L., 1983. Observations of near-surface currents and temperature in the central and western tropical Atlantic Ocean. *J. Geophys. Res.* 88, 4433–4438. <https://doi.org/10.1029/JC088iC07p04433>.
- Nascimento, R.A., Johnstone, H.J.H., Kuhnert, H., Santos, T.P., Venancio, I.M., Chiessi, C.M., Ballalai, J.M., Campos, M.C., Govin, A., Mulitza, S., Albuquerque, A.L.S., 2023. Long-term variability of the western tropical Atlantic sea surface temperature driven by greenhouse gases and AMOC. *Quat. Sci. Rev.* 322, 108431. <https://doi.org/10.1016/j.jqr.2023.108431>.
- North Greenland Ice Core Project members, 2004. High-resolution record of Northern Hemisphere climate extending into the last interglacial period. *Nature* 431, 147–151. <https://doi.org/10.1038/nature02805>.
- Nürnberg, D., Müller, A., Schneider, R.R., 2000. Paleo-sea surface temperatures and Mg/Ca ratios of sediment core GeoB1112-4. <https://doi.org/10.1594/PANGAEA.710811>.
- Oppo, D.W., Curry, W.B., McManus, J.F., 2015. What do benthic δ<sup>13</sup>C and δ<sup>18</sup>O data tell us about Atlantic circulation during Heinrich Stadial 1? *Paleoceanography* 30, 353–368. <https://doi.org/10.1002/2014PA002667>.
- Osman, M.B., Tierney, J.E., Zhu, J., Tardif, R., Hakim, G.J., King, J., Poulsen, C.J., 2021. Globally resolved surface temperatures since the last glacial maximum. *Nature* 599, 239–244. <https://doi.org/10.1038/s41586-021-03984-4>.
- Pedro, J.B., Jochum, M., Buizert, C., He, F., Barker, S., Rasmussen, S.O., 2018. Beyond the bipolar seesaw: toward a process understanding of interhemispheric coupling. *Quat. Sci. Rev.* 192, 27–46. <https://doi.org/10.1016/j.jqr.2018.05.005>.
- Peltier, C., Kaplan, M.R., Birkel, S.D., Soteres, R.L., Sagredo, E.A., Aravena, J.C., Araos, J., Moreno, P.I., Schwartz, R., Schaefer, J.M., 2021. The large MIS 4 and long

- MIS 2 glacier maxima on the southern tip of South America. *Quat. Sci. Rev.* 262, 106858. <https://doi.org/10.1016/j.quascirev.2021.106858>.
- Peterson, R.G., Stramma, L., 1991. Upper-level circulation in the South Atlantic Ocean. *Prog. Oceanogr.* 26, 1–73. [https://doi.org/10.1016/0079-6611\(91\)90006-8](https://doi.org/10.1016/0079-6611(91)90006-8).
- Philander, S.G., 2001. Atlantic Ocean equatorial currents. In: *Encyclopedia of Ocean Sciences*. Elsevier, pp. 188–191. <https://doi.org/10.1006/rwos.2001.0361>.
- Philander, S.G.H., Pacanowski, R.C., 1986. A model of the seasonal cycle in the tropical Atlantic Ocean. *J. Geophys. Res.* 91, 14192–14206. <https://doi.org/10.1029/JC091iC12p14192>.
- Pinho, T.M.L., Yang, H., Lohmann, G., Portilho-Ramos, R.C., Chiessi, C.M., Bahr, A., Nürnberg, D., Repschläger, J., Shi, X., Tiedemann, R., Mulitza, S., 2025. Asynchronous poleward migration of the Atlantic subtropical gyres over the past 22,000 years. *Geophys. Res. Lett.* 52, e2024GL111497. <https://doi.org/10.1029/2024GL111497>.
- Richardson, P.L., Reverdin, G., 1987. Seasonal cycle of velocity in the Atlantic North Equatorial Counter-current as measured by surface drifters, current meters, and ship drifts. *J. Geophys. Res.* 92, 3691–3708. <https://doi.org/10.1029/JC092iC04p03691>.
- Pokras, E.M., Mix, A.C., 1987. Earth's precession cycle and Quaternary climatic change in tropical Africa. *Nature* 326, 486–487. <https://doi.org/10.1038/326486a0>.
- Richardson, P.L., Arnault, S., Garzoli, S., Bruce, J.G., 1992. Annual cycle of the Atlantic North Equatorial Countercurrent. *Deep-Sea Res., Part A* 39, 997–1014. [https://doi.org/10.1016/0198-0149\(92\)90036-S](https://doi.org/10.1016/0198-0149(92)90036-S).
- Richey, J.N., Thirumalai, K., Khider, D., Reynolds, C.E., Partin, J.W., Quinn, T.M., 2019. Considerations for Globigerinoides ruber (white and pink) paleoceanography: comprehensive insights from a long-running sediment trap. *Paleoceanogr. Paleoclimatol.* 34, 353–373. <https://doi.org/10.1029/2018PA003417>.
- Rodrigues, R.R., Rothstein, L.M., Wimbush, M., 2007. Seasonal variability of the south equatorial current bifurcation in the Atlantic Ocean: a numerical study. *J. Phys. Oceanogr.* 37, 16–30. <https://doi.org/10.1175/JPO2983.1>.
- Rosenthal, Y., Linsley, B., 2007. PALEOCEANOGRAPHY, PHYSICAL AND CHEMICAL PROXIES | Mg/Ca and Sr/Ca paleothermometry. In: *Encyclopedia of Quaternary Science*. Elsevier, pp. 1723–1731. <https://doi.org/10.1016/B0-44-452747-8/00306-9>.
- Santos, T.P., Lessa, D.O., Venancio, I.M., Chiessi, C.M., Mulitza, S., Kuhnert, H., Govin, A., Machado, T., Costa, K.B., Toledo, F., Dias, B.B., Albuquerque, A.L.S., 2017. Prolonged warming of the Brazil current precedes deglaciations. *Earth Planet Sci. Lett.* 463, 1–12. <https://doi.org/10.1016/j.epsl.2017.01.014>.
- Santos, T.P., Shimizu, M.H., Nascimento, R.A., Venancio, I.M., Campos, M.C., Portilho-Ramos, R.C., Ballalai, J.M., Lessa, D.O., Crivellari, S., Nagai, R.H., Chiessi, C.M., Kuhnert, H., Bahr, A., Albuquerque, A.L.S., 2022. A data-model perspective on the Brazilian margin surface warming from the last glacial maximum to the Holocene. *Quat. Sci. Rev.* 286, 107557. <https://doi.org/10.1016/j.quascirev.2022.107557>.
- Schmidt, M.W., Spero, H.J., Lea, D.W., 2004. (Table SI-2) stable oxygen isotope and Mg/Ca ratios of Globigerinoides ruber from ODP hole 165-999A. <https://doi.org/10.1594/PANGAEA.716694>.
- Shackleton, S., Menking, J.A., Brook, E., Buzert, C., Dyonisius, M.N., Petrenko, V.V., Baggenstos, D., Severinghaus, J.P., 2021. Evolution of mean ocean temperature in marine isotope stage 4. *Clim. Past* 17, 2273–2289. <https://doi.org/10.5194/cp-17-2273-2021>.
- Schaefer, J.M., Putnam, A.E., Denton, G.H., Kaplan, M.R., Birkel, S., Doughty, A.M., Kelley, S., Barrell, D.J.A., Finkel, R.C., Winckler, G., Anderson, R.F., Ninneman, U.S., Barker, S., Schwartz, R., Andersen, B.G., Schuechter, C., 2015. The Southern glacial maximum 65,000 years ago and its unfinished termination. *Quat. Sci. Rev.* 114, 52–60. <https://doi.org/10.1016/j.quascirev.2015.02.009>.
- Shi, N., Schneider, R., Beug, H.-J., Dupont, L.M., 2001. Southeast trade wind variations during the last 135 kyr: evidence from pollen spectra in eastern South Atlantic sediments. *Earth and Planetary Science Letters* 187, 311–321. [https://doi.org/10.1016/S0012-821X\(01\)00267-9](https://doi.org/10.1016/S0012-821X(01)00267-9).
- Schlitzer, R. 2023. Ocean Data View, ody.awi.de.
- Sigman, D.M., Boyle, E.A., 2000. Glacial/interglacial variations in atmospheric carbon dioxide. *Nature* 407, 859–869. <https://doi.org/10.1038/35038000>.
- Skonieczny, C., McGee, D., Winckler, G., Bory, A., Bradtmiller, L.I., Kinsley, C.W., Polissar, P.J., De Pol-Holz, R., Rossignol, L., Malaizé, B., 2019. Monsoon-driven Saharan dust variability over the past 240,000 years. *Sci. Adv.* 5, eaav1887. <https://doi.org/10.1126/sciadv.aav1887>.
- Stocker, T.F., Johnsen, S.J., 2003. A minimum thermodynamic model for the bipolar seesaw. *Paleoceanography* 18, 2003PA000920. <https://doi.org/10.1029/2003PA000920>.
- Stramma, L., England, M., 1999. On the water masses and mean circulation of the South Atlantic Ocean. *J. Geophys. Res.* 104, 20863–20883. <https://doi.org/10.1029/1999JC000139>.
- Stuut, J.-B.W., Prins, M.A., Schneider, R.R., Weltje, G.J., Jansen, J.H.F., Postma, G., 2002. A 300-kyr record of aridity and wind strength in southwestern Africa: inferences from grain-size distributions of sediments on Walvis Ridge, SE Atlantic. *Mar. Geol.* 180, 221–233. [https://doi.org/10.1016/S0025-3227\(01\)00215-8](https://doi.org/10.1016/S0025-3227(01)00215-8).
- Venancio, I.M., Mulitza, S., Govin, A., Santos, T.P., Lessa, D.O., Albuquerque, A.L.S., Chiessi, C.M., Tiedemann, R., Vahlenkamp, M., Bickert, T., Schulz, M., 2018. Millennial- to orbital-scale responses of Western equatorial Atlantic thermocline depth to changes in the trade wind system since the last interglacial. *Paleoceanogr. Paleoclimatol.* 33, 1490–1507. <https://doi.org/10.1029/2018PA003437>.
- Venancio, I.M., Shimizu, M.H., Santos, T.P., dos, Lessa, D.O., Dias, B.B., Chiessi, C.M., Mulitza, S., Kuhnert, H., Tiedemann, R., Vahlenkamp, M., Bickert, T., Belem, A.L., Sampaio, G., Albuquerque, A.L.S., Nobre, C., 2021. High-resolution SST records derived from planktonic foraminiferal Mg/Ca from the western equatorial Atlantic 2 datasets. <https://doi.org/10.1594/PANGAEA.931646>.
- Wang, X., Auler, A.S., Edwards, R.L., Cheng, H., Cristalli, P.S., Smart, P.L., Richards, D.A., Shen, C.-C., 2004. Wet periods in northeastern Brazil over the past 210 kyr linked to distant climate anomalies. *Nature* 432, 740–743. <https://doi.org/10.1038/nature03067>.
- Weldeab, S., Lea, D.W., Schneider, R.R., Andersen, N., 2007. 155,000 years of West African monsoon and ocean thermal evolution. *Science* 316, 1303–1307. <https://doi.org/10.1126/science.1140461>.
- Wolff, T., Mulitza, S., Röhle, C., Wefer, G., 1999. Response of the tropical Atlantic thermocline to late Quaternary trade wind changes. *Paleoceanography* 14, 374–383. <https://doi.org/10.1029/1999PA900011>.
- Yu, J., Menivel, L., Jin, Z.D., Thornalley, D.J.R., Barker, S., Marino, G., Rohling, E.J., Cai, Y., Zhang, F., Wang, X., Dai, Y., Chen, P., Broecker, W.S., 2016. Sequestration of carbon in the deep Atlantic during the last glaciation. *Nat. Geosci.* 9, 319–324. <https://doi.org/10.1038/ngeo2657>.
- Zarriess, M., Johnstone, H.J.H., Prange, M., Steph, S., Groeneveld, J., Mulitza, S., Mackensen, A., 2011. Sea surface temperature reconstruction based on the Mg/Ca ratio of planktonic Foraminifera Globigerinoides ruber pink in sediment profile GeoB9526. <https://doi.org/10.1594/PANGAEA.756440>.